ORIGINAL ARTICLE

Cadmium free Cu_2ZnSnS_4 solar cells with 9.7 % efficiency

J. K. Larsen[1] | F. Larsson[1] | T. Törndahl[1] | N. Saini[1] | L. Riekehr[1] | Y. Ren[1,‡] | A. Biswal[2,3] | D. Hauschild[2,3] | L. Weinhardt[2,3,4] | C. Heske[2,3,4] | C. Platzer-Björkman[1]

[1]Ångström Solar Center, Division of Solid State Electronics, Ångström Laboratory, Uppsala University, Uppsala 752 36, Sweden

[2]Institute for Photon Science and Synchrotron Radiation (IPS), Karlsruhe Institute of Technology (KIT), Hermann-v.-Helmholtz-Platz 1, 76344 Eggenstein-Leopoldshafen, Germany

[3]Institute for Chemical Technology and Polymer Chemistry (ITCP), Karlsruhe Institute of Technology (KIT), Engesserstr. 18/20, 76128 Karlsruhe, Germany

[4]Department of Chemistry and Biochemistry, University of Nevada, Las Vegas (UNLV), 4505 Maryland Parkway, Las Vegas, NV 89154-4003, USA

Correspondence
Ångström Solar Center, Division of Solid State Electronics, Ångström Laboratory, Uppsala University, Uppsala 752 36, Sweden
Email: jes.larsen@angstrom.uu.se

Present address
‡Midsummer AB, Electronikhöjden 6, 175 43 Järfälla, Sweden

Cu_2ZnSnS_4(CZTS) thin-film solar cell absorbers with different band gaps can be produced by parameter variation during thermal treatments. Here, the effects of varied annealing time in sulfur atmosphere and an ordering treatment of the absorber are compared. Chemical changes in the surface due to ordering are examined, and a downshift of the valence band edge is observed. With the goal to obtain different band alignments these CZTS absorbers were combined with $Zn_{1-x}Sn_xO_y$ (ZTO) or CdS buffer layers to produce complete devices. A high open circuit voltage of 809 mV is obtained for an ordered CZTS absorber with CdS buffer layer, while a 9.7% device is obtained utilizing a Cd free ZTO buffer layer. The best performing devices are produced with a very rapid 1 min sulfurization, resulting in very small grains.

KEYWORDS
Thin film solar cells, Cu_2ZnSnS_4, thermal treatment, valence band

Funding information
Financial support from the Swedish Energy Agency [grant number 2017-004796], StandUp for Energy,and the Swedish Foundation for Strategic Research projects RMA15-0030 and FFL12-0178 are gratefully acknowledged

1 | INTRODUCTION

Cu_2ZnSnS_4 (CZTS) has received substantial interest as a potential material for photovoltaic applications in recent years. The material is primarily interesting, since it consists of earth abundant and non-toxic elements. The highest efficiency demonstrated for CZTS to date is 11% [1]. For this record efficiency a CdS/CZTS stack underwent a heat treatment, leading to inter-diffusion at the interface. It was argued that a new phase forms during the heat treatment near the absorber/buffer interface, which modifies the band alignment [1]. The importance of the conduction band offset (CBO) at the absorber/buffer interface is well known [2, 3]. A cliff structure (CBO<0) can lead to detrimental interface recombination, while a large spike results in blocking of the photocurrent and reduced fill factor [2]. A flat conduction band alignment (CBO $\sim$ 0) is usually found in high-efficiency Cu(In,Ga)Se_2 devices [4, 5]. A direct determination of the CBO at the CdS/CZTS interface revealed a significant cliff of -0.34 eV [6], while other studies report CBOs ranging from a spike of 0.41eV to a cliff of -0.34 eV[6, 7, 8]. Commonly, it is assumed that a small cliff is present at the CZTS/CdS interface, which highlights the need to replace CdS with materials with a higher conduction band minimum in order to avoid an unfavorable band alignment [9].

The band alignment between the buffer layer and CZTS has been studied for various buffer layer systems such as CdS [6, 10], $ZnO_{1-x}S_x$ [10], In_2S_3 [10], and $Zn_{1-x}Cd_xS$ [11]. In our previous work, we have focused on $Zn_{1-x}Sn_xO_y$ (ZTO) buffer layers deposited by atomic layer deposition (ALD) as an alternative to CdS for CZTS [12, 13] and Cu(In,Ga)Se_2 (CIGS) [14, 15]. It has been demonstrated that the ZTO band gap can be tuned by adjustment of the ALD growth temperature. Growth temperatures in the range of 90–180 °C resulted in ZTO films with band gaps in the range of 3.25 - 3.75 eV [14], and it is assumed that this affects the CBO as well. Recently it was reported that an ultrathin Zn(O,S) layer is formed at the ZTO/CZTS interface, which might reduce interface recombination, and be one reason for good efficiencies achieved with this buffer layer [16].

Several studies show that the apparent bulk band gap of CZTS is strongly affected by both the annealing conditions and post annealing ordering treatments [17, 18, 19]. When the Cu-Zn order in CZTS is increased, the band gap is widened significantly [17, 19, 20, 21]. Since the band alignment with CdS is assumed to be cliff-like, this cliff would presumably worsen in ordered CZTS if the conduction band shifts up relative to the buffer. Thus, a better suited buffer layer can possibly unlock the potential of the higher band gap of ordered CZTS. In this work, we investigate how the surface valence band edges and the bulk band gap of CZTS can be varied, leading to both high efficiencies and high open circuit voltages.

2 | EXPERIMENTAL

In this work 1 mm soda lime glass substrates were coated with 300 nm Mo by DC sputtering. Cu-Zn-Sn-S precursors were deposited by sputtering from binary CuS, ZnS, and SnS targets in an argon atmosphere. The composition of the precursors was measured by X–ray fluorescence. Two batches of precursors were used in this work. Samples for UPS/XPS measurements had the composition ratios Cu/Sn = 1.89 and Zn/(Cu+Sn) = 0.33 while precursors with composition ratios of Cu/Sn = 1.89 and Zn/(Cu+Sn) = 0.38 were used for the devices.

Sulfurization of the precursors was performed in a pyrolytic carbon coated graphite box containing 70 mg of elemental sulfur. The graphite box was introduced into a preheated tube furnace with an argon background pressure of 350 Torr. When samples were transferred to the hot zone the temperature of the box increased to 580 °C in about 90 s. The samples were allowed to dwell for either 1 or 13 minutes. For a more detailed description of the annealing process see reference [22]. Samples for device fabrication were exposed to an air annealing treatment after sulfurization. This

was done by placing the sample onto a preheated hotplate set to 300 °C for 80 seconds. After removing the samples, the temperature of the hotplate was reduced to 200 °C and the samples were air annealed for additionally 10 min. After the air annealing treatment the samples were removed from the hot plate and allowed to cool to room temperature.

Some samples underwent an ordering treatment. This was done by heating the samples to 300 °C in an argon atmosphere. The samples were then slowly cooled to room temperature with a rate of 0.1 °C/min. The ordering treatment was always performed after air annealing, but before deposition of the buffer layer. The samples that did not undergo an ordering treatment are referred to as "disordered", but will have some degree of ordering determined by the cooling rate after air annealing.

Before buffer layer deposition, the absorbers were etched for 2 min in 5% KCN. Subsequently, either CdS was deposited by chemical bath deposition or ZTO by atomic layer deposition (ALD). About 60 nm of CdS is deposited by chemical bath deposition at 60 °C following the procedure described in [23]. The $Zn_{1-x}Sn_xO_y$ films were grown in an F-120 Microchemistry reactor at 120 °C. In total 1000 cycles were deposited using a 1:1 ZnO:SnO_2 super cycle approach with pulse lengths of 0.4:0.8:0.4:0.8 s for DEZn/TDMASn:N_2:H_2O:N_2, respectively [14]. Using the same process parameters, the corresponding thickness and composition (x-value) for a 500 cycles film on a soda lime glass substrate were measured by XRF to be 28 nm and x=0.18, respectively. A band gap of the ZTO film of 3.6 eV is estimated from transmission-reflection measurements on similar samples on quartz substrates.

The devices were completed by sputter deposition of an i-ZnO/Al:ZnO bilayer and mechanical scribing to define cells with an area of 0.05 cm^2. Dark and illuminated JV measurements were performed with a Newport ABA solar simulator and the external quantum efficiency (QE) was measured in a homebuilt setup. For calculation of the internal QE, the reflectance was measured with a Bentham PVE300 system.

Photoluminescence (PL) and Raman measurements were performed at room temperature in a Renishaw inVia confocal Raman microscope equipped with an InGaAs and Si CCD detector using 785 and 532 nm lasers. To perform Raman measurement on the back contact after device completion the absorbers were delaminated. A piece of glass was glued onto the device stack with superglue. When removing the glass with force, the device delaminated at the Mo/CZTS interface.

Cross-section transmission electron microscope (TEM) lamellas were prepared with a focused ion beam and scanning electron microscope (FIB-SEM, FEI Strata DB235). The in-situ lift out technique was used and the TEM lamella was attached to a Ti grid. The TEM lamella was then polished to electron transparency and a final Ga ion beam treatment with an energy of 5 kV was used for removing the amorphized surface layer. For TEM analysis, a probe corrected FEI Titan Themis equipped with the SuperX system for energy dispersive X-ray spectroscopy (EDX) and operated at 200 kV was used.

For photoelectron spectroscopy measurements, the absorber samples (i.e., after the KCN etch) were sealed in a plastic bag under inert gas and shipped to KIT. At KIT, the samples were transferred into the UHV system via a glovebox without any additional ambient air exposure. The UHV analysis chamber is equipped with an Omicron Argus CU electron analyzer, a DAR450 twin anode x-ray source generating Mg Kα and Al Kα x-rays for XPS, and a He gas discharge lamp for He II UPS.

3 | RESULTS AND DISCUSSION

The results of this work are separated into three sections: Section 3.1 discusses how the bulk band gap of CZTS can be modified depending on the annealing conditions. Section 3.2 reports on the changes in chemical and electronic structure at the absorber surface as a result of different thermal treatments. Finally in section 3.3, the influence of the

different preparation parameters on the final device is investigated.

3.1 | Effect of ordering and annealing time on the band gap of Cu_2ZnSnS_4

In this section, it is discussed how the band gap of CZTS can be modified by the annealing conditions. Two different approaches will be shown to affect the apparent band gap extracted from internal quantum efficiency (IQE). For this purpose, samples annealed in a sulfur containing atmosphere for 1 minute are compared to samples annealed for 13 minutes (denoted "D1/CdS", and "D13/CdS"). It has previously been observed that the annealing time affects the apparent band gap in our process due to loss of sulfur from the graphite box [17]. These devices are compared to two samples annealed in sulfur followed by a slow cooling ordering treatment (labeled “O1/CdS” and “O13/CdS” after 1 and 13 min annealing, resp.).

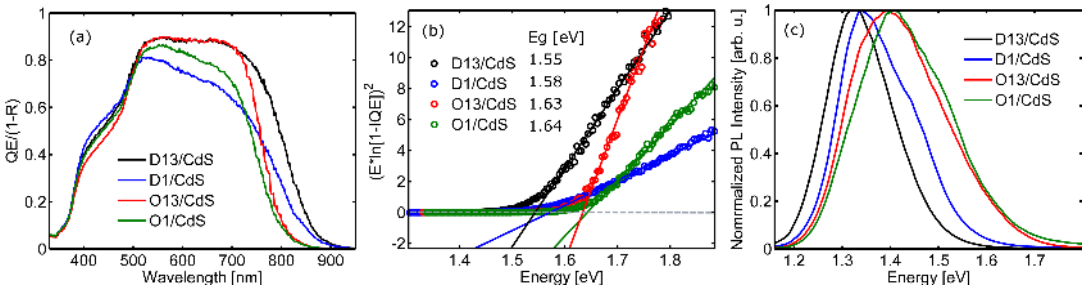

FIGURE 1 (a) Internal quantum efficiency of devices processed under different conditions. D13/CdS and D1/CdS were annealed for 13 and 1 min respectively. The samples O1/CdS and O13/CdS were annealed like D1/CdS and D13/CdS and subsequently ordered with a slow cooling treatment. (b) Determination of the band gaps from a linear extrapolation (fit) of the leading edge in the spectrum. (c) Room temperature photoluminescence of the same devices.

Figure 1 shows the quantum efficiency and photoluminescence of the devices. In order to extract the band gap energy from QE measurements, we employ the method described by Richter et al. [24]. The internal quantum efficiency (IQE) is determined by the collection efficiency and the absorption characteristics of the solar cell. For absorbers thicker than $W + L_D$, where W is the width of the space charge region, and L_D is the effective carrier diffusion length, the internal quantum efficiency is given by [25]:

$$IQE = 1 - \frac{\exp(-\alpha W)}{\alpha L_D + 1}, \tag{1}$$

where α is the absorption coefficient. Assuming that the product $\alpha L_D << 1$, equation 1 can be rearranged to:

$$\alpha(h\nu) \propto -ln(1 - IQE(h\nu)). \tag{2}$$

This approximation is only valid in the region where α is small, for example the weakly absorbing tail states below E_g, or in material with a short diffusion length. According to Gokmen et al. this approximation is valid for IQE<0.3, where α is considered sufficiently small [26] . For a direct band gap semiconductor the absorption coefficient is described by the square root behavior: $\alpha = \frac{A_0}{h\nu}\sqrt{E_g - h\nu}$, where A_0 is a constant. The x-intercept of the linear fit of $(h\nu ln[1 - IQE])^2$

versus photon energy can be used to estimate the band gap energy [24].

For sample D13/CdS, which represents the anneal for 13 minutes in sulfur, we derive a band gap of 1.55 eV. When reducing the annealing time to 1 minute, a small increase to 1.58 eV is observed. Note, however, that the 1 min anneal results in devices with poorer collection resulting in lower QE. Since the reduced collection efficiency can result in a lower extracted band gap [27], it is important to be cautious when interpreting the band gap change. An error bar of the fit of the order of ± 0.05 eV, which is estimated by variation of the number of included data points within acceptable boundaries, must also be taken into account. In order to verify that the change in band gap is not only related to the change in collection efficiency, photoluminescence measurements of the devices are included in Figure 1(c). A small blue shift of about 30 meV is observed for the 1 min annealed sample compared to the 13 min sample. This indicates that the band gap widening extracted from IQE is not entirely dominated by collection, but a small band gap shift is in fact caused by the change in annealing time. This difference is smaller than the impact of annealing time observed previously [17]. It is worth noticing that the PL peak maximum is about 230 mV lower than the band gap extracted from IQE. It has been suggested that the low energy of the PL peak is a result of a very high density of defect states near the band edges or formation of stannite inclusions [28]. The low energy of the PL emission has also been tied to tail states arising from electrostatic potential fluctuations due to high compensation [26].

Ordering of a set of samples with a slow cooling treatment results in further band gap widening up to 1.64 eV in the case of O1/CdS. When comparing the baseline samples (D13/CdS and D1/CdS) with the ordered samples (O13/CdS and O1/CdS) it is noticed that the IQE is similar or higher for intermediate wavelengths in ordered samples. Therefore, the band gap increase relative to the the baseline samples, is not the result of poorer charge carrier collection, but rather a real band gap widening. This is again confirmed with PL, where the maximum is shifted by about 80 meV compared to D13/CdS. The band gap widening can be attributed to an increased cation order in CZTS [19] based on Raman spectroscopy performed with a 785 nm laser. The order parameter, which is defined as the ratio of the peak heights of the 289 and 305 cm^{-1} peaks (Q= H289/H305) describes the Cu-Zn disorder in the material [29, 18]. For these samples an ordering parameter of Q = 2.35 is found for O1/CdS compared to Q = 0.66 for D13/CdS.

3.2 | Chemical and electronic structure of Cu_2ZnSnS_4 absorbers

To investigate the impact of the thermal treatment on the chemical and electronic structure, surface-sensitive XPS and UPS measurements with a characteristic attenuation length (inelastic mean free path, IMFP) of $\lambda \approx$ 1-3 nm were performed. Figure 2 shows the XPS survey spectra of the CZTS samples, annealed for 1 and 13 minutes and with and without ordering treatment.

The XPS survey spectra of all four samples show strong intensities for the copper, zinc, tin, and sulfur-related peaks, as expected. We find that the Zn 2p peaks of the ordered samples have a significantly higher intensity. In parallel, the Cu 2p intensity of the ordered samples is slightly below those of the disordered samples, while the Sn 3d peak intensity remains constant. We have calculated the Zn/Sn ratio using the Zn 3d and Sn 4d peaks; these photoemission lines have similar kinetic energies and thus almost identical IMFP and analyzer transmission. Accordingly, the Zn/Sn ratio can be derived solely using the peak intensities and corresponding photoionization cross sections [30]. We find that the disordered and ordered absorber samples have a Zn/Sn ratio of 1.0 and 1.3 (±0.05), respectively. In addition, a minor O 1s signal and a small C 1s signal indicate a low amount of surface adsorbates.

To investigate the impact of the different treatments on the valence band maximum, Figure 3 shows the UPS valence band spectra of the CZTS absorbers annealed for 1 and 13 min with and without ordering treatment, respectively. The valence band maximum (VBM) is determined with a linear extrapolation of the leading edge of the valence band [31]. The approximations in this approach [31] lead to an absolute error of the VBM position of ± 0.1 eV, while relative changes

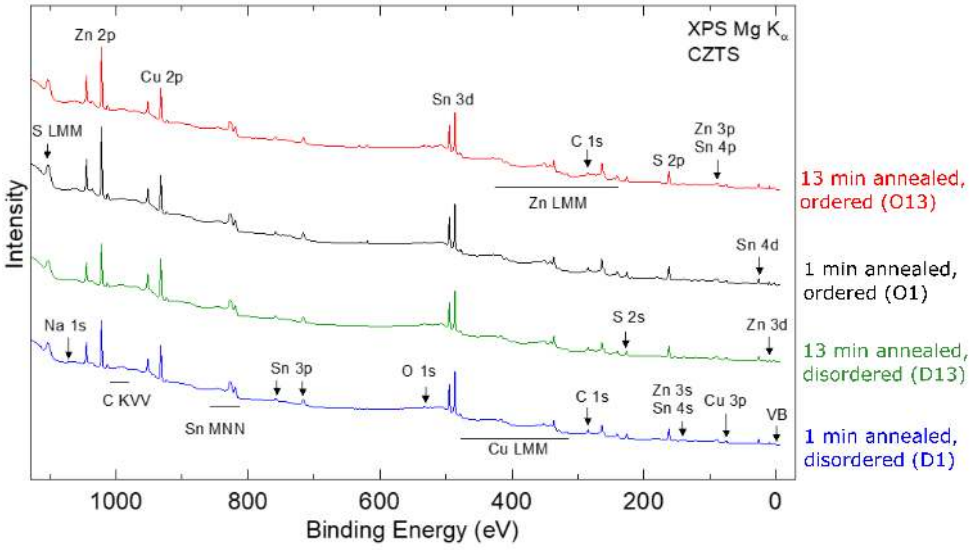

FIGURE 2 Mg K_α-excited XPS survey spectra of four CZTS samples, which underwent different annealing times with and without ordering treatment. Prominent photoemission peaks and Auger features are labeled.

only depend on the uncertainty of the fit and can be determined with higher precision. Disordered and ordered samples show a similar spectral shape. For the ordered samples, the feature at ~ 3 eV which is attributed to Cu 3d-derived states, is less intense than for the disordered samples, which can likely be explained with a copper reduction at the surface of the ordered absorbers (corroborated by the XPS results). The disordered samples show a VBM of -0.77 and -0.71 eV for the 1 and 13 min annealed sample, respectively. After the ordering treatment, the VBM significantly shifts downwards (i.e., away from the Fermi level) to -0.89 eV, independent of the sulfurization annealing time.

We note that the VBM shift at the surface is significantly larger than the changes of the bulk band gap discussed above. In addition to an increase of the electronic surface band gap, this could also be due to an overall downward shift of all electronic levels. In case of such a band bending, a rigid shift of all core-level lines in parallel with the VBM would also be expected. Analyzing the (relative) shifts of the Zn $2p_{3/2}$ and Cu $2p_{3/2}$ lines, we find that the variation from one sample to another is much smaller (in the range of up to +70 meV) than the VBM shift and in the opposite direction. Thus, it is more likely that the changes in surface composition, in particular the reduced Cu content after the ordering treatment, leads to a widening of the band gap at the absorber surface. An earlier study showed that the difference in surface to bulk composition can indeed lead to an increased band gap at the surface compared to the bulk [6].

3.3 | Devices with different Cu_2ZnSnS_4 band gaps

It was demonstrated that the bulk and surface band gaps of CZTS can be modified by the choice of process conditions. In the following, we investigate the influence of these process conditions on the parameters of the final devices. Figure 4 shows the JV curves for devices annealed for either 1 or 13 min, either ordered or disordered. For each case CdS buffer layers are compared to ZTO. The samples are named according to the system:(D: disordered, O: ordered)(annealing time in minutes)/(CdS, ZTO). Table 1 shows the device parameters of the best device as well as the average and standard deviation obtained from 20 devices on each sample.

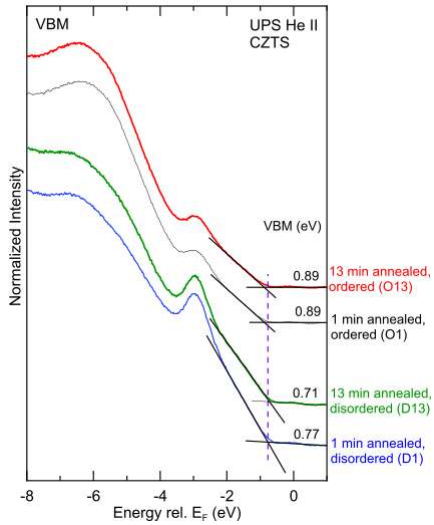

FIGURE 3 He II UPS spectra of the valence band. The VBM position with respect to the Fermi energy is determined by a linear extrapolation of the leading edge. The dotted line represents the VBM position for the 1min annealed, disordered CZTS absorber (0.77 eV).

From these 8 different device fabrication routes some trends are observed. In general, the ordering treatment leads to an increased V_{OC}, for devices that do not show a blocking behavior in the IV curve. This agrees with the widened band gap, and is in line with the results of earlier studies [17, 32]. Two devices, in particular, are worth highlighting. The 1 min annealed sample with ordering treatment (O1/CdS) has a record high V_{OC} of 809 mV after deposition of a MgF_2 antireflective coating. This is to our knowledge among the highest open circuit voltage obtained for CZTS. The highest V_{OC} previously reported for a CZTS device are 783 mV [17] and 784mV [32]. Both of these results were obtained after an ordering treatment of CZTS. The other sample, which stands out is D1/ZTO - a result of 1 min annealing, and use of ZTO buffer layer. After deposition of AR coating, a device efficiency of 9.7% is obtained. This is the highest efficiency of CZTS with a Cd-free buffer layer to date.

Another observation is the large effect that the annealing duration has on device properties. By comparing the ordered samples with CdS buffer layers O13/CdS and O1/CdS, the 1 min annealed sampled resulted in a V_{OC} of 801 mV, whereas the 13 min sample had a V_{OC} of 718 mV. The studies of the surface composition and valence band position in section 3.2 indicated that the surfaces of the two ordered absorber samples are not significantly different. The V_{OC} difference is therefore unlikely to be a simple consequence of the surface condition. Rather, we speculate that the V_{OC} difference highlights the important role of the sulfurization for the performance of the material. It appears that the shorter annealing, during which the sulfur partial pressure was kept high, resulted in material with better bulk properties, which could be due to the formation of fewer detrimental defects during the exposure to a higher sulfur partial pressure.

It has previously been demonstrated that CZTS with a ZTO buffer layer can outperform CdS devices, provided that the properties of the ZTO layer are tuned appropriately [13, 12, 16]. Since growth temperature and composition affects the band gap, it is necessary to tune the growth conditions to obtain an optimized band alignment [12]. The reason for the enhanced performance using ZTO instead of CdS is possibly due to reduced interface recombination because of either better band alignment [13] or formation of a Zn(O,S) passivating tunnel layer [16]. Reduced parasitic absorption

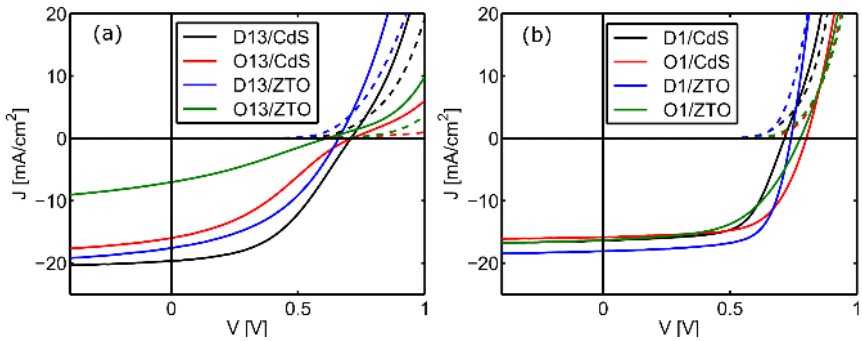

FIGURE 4 JV characteristics of the best device from each sample. The following naming is used: (D: disordered, O: ordered)(annealing time)/(CdS, ZTO) (a) Devices resulting from 13 min annealing, (b) Devices resulting from 1 min annealing.

furthermore gives a slightly increased J_{SC}. The benefit of ZTO was however not clearly seen for all devices presented in this study. The only device that demonstrated a benefit of ZTO was the 1 min annealed disordered sample with a band gap of 1.59 eV. For all other devices shown here the V_{OC} and efficiency of the ZTO devices were lower than the CdS references. Since both lower band gap absorbers (1.55 eV) and higher band gap absorbers (1.64 eV) did not benefit from the ZTO buffer layer, it is likely that the CB alignments cannot explain the different device performances alone.

The short 1 min anneal resulted in devices that perform better than the baseline 13 min anneal. One reason for this is that devices annealed for 13 minutes tend to show a kink in the JV curves (i.e., a blocking behavior), which could be related to the back contact [21]. Malerba et al. reported that a band gap widening of 170 mV due to CZTS ordering could result in blocking that, in turn, is explained by a back contact barrier [21]. Their model assumes that the VB is shifted down by the same amount as the band gap widening.

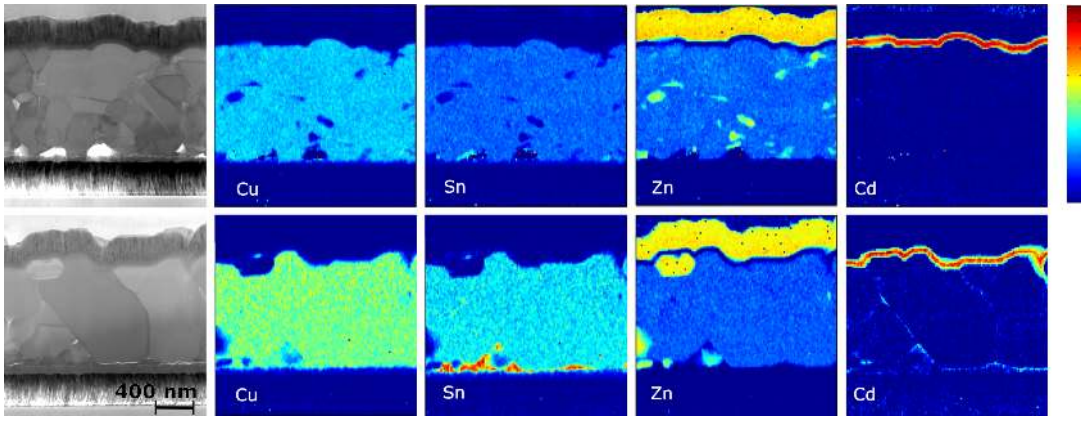

FIGURE 5 TEM and EDS measurements of D1/CdS, an 1 min annealed CZTS device (top row) and D13/CdS, a 13 min annealed sample (bottom row). In EDS measurements the top of the color bar in the right (red) represents high relative concentration, while the bottom (blue) represents low relative concentration.

To further shed light on the blocking behavior of the 13 min annealed devices, the micro-structure is analyzed by

Sample name	Eg [eV]	V_{OC} [mV]	J_{SC} [mA/cm^2]	FF [%]	Eff [%]
D1/CdS	1.58	715 *(708 ± 10)*	16.4 *(15.6 ± 0.6)*	64 *(62.4 ± 3.4)*	7.5 *(6.9 ± 0.4)*
D1/ZTO	1.59	740 *(731 ± 9)*	18.1 *(17.2 ± 0.8)*	68.8 *(65.1 ± 3.9)*	9.2 *(8.2 ± 0.9)*
O1/CdS	1.64	801 *(792 ± 8)*	15.8 *(15.6 ± 0.3)*	64.8 *(61.6 ± 2.7)*	8.2 *(7.6 ± 0.4)*
O1/ZTO	1.65	778 *(776 ± 17)*	16.3 *(16.2 ± 0.5)*	56.4 *(50.3 ± 3.4)*	7.1 *(6.3 ± 0.6)*
D13/CdS	1.55	709 *(699 ± 24)*	19.4 *(19.3 ± 0.3)*	47.1 *(44.4 ± 1.7)*	6.5 *(6.0 ± 0.3)*
D13/ZTO	1.55	659 *(656 ± 4)*	17.8 *(17.1 ± 0.4)*	43.9 *(39.6 ± 1.9)*	5.1 *(4.4 ± 0.3)*
O13/CdS	1.63	718 *(695 ± 42)*	15.9 *(15.2 ± 0.8)*	34.5 *(33.0 ± 1.7)*	3.9 *(3.5 ± 0.4)*
O13/ZTO	1.62	612 *(540 ± 35)*	7.0 *(5.6 ± 0.5)*	29.6 *(30.2 ± 0.4)*	1.3 *(0.9 ± 0.1)*
D1/ZTO*		746	19.1	68.0	9.7
O1/CdS*		809	17.0	61.2	8.4

TABLE 1 Comparison of the devices from each sample annealed for either 1 or 13 minutes. Samples that underwent an ordering treatment are labeled (O), while disordered samples are labeled (D). For each thermal treatment CdS and ZTO buffer layers are compared. The table shows the parameters for the best device followed the average value of each parameter (*average ± standard deviation*) obtained from measurement of 20 cells on each sample. *Best device after deposition of antireflective MgF_2 coating.

TEM measurements. Figure 5 shows the resulting cross sections of a 1 and 13 min annealed absorber after device finishing with CdS buffer layers (D13/CdS and D1/CdS). The grains are significantly smaller after 1 min of sulfurization compared to after 13 min, where grain sizes approach the film thickness. Also small voids are observed in the 1 min sample. This could be a result of preferential sputtering of ZnS when preparing the TEM lamellas [33]. It is noticed that the MoS_2 interlayer formed at the Mo/CZTS interface is thicker in the 13 min sample than in the 1 min sample. This could have a detrimental effect on the device performance [34, 35, 36]. The degree to which the MoS_2 layer is detrimental is, however, not fully understood. It should be noted that the record efficiency CZTS devices had an almost 200 nm thick MoS_2 interface layer, and did not suffer from low FF due to hole blocking [1]. The MoS_2 could still contribute to increased series resistance. Zn- and Sn-rich regions are observed in both samples (presumably secondary ZnS and SnS_2 phases, respectively). The Zn-rich regions are small and distributed throughout the layer after 1 min of annealing, and form larger regions either at the surface or near the back contact after longer annealing times. Sn-rich regions are primarily seen at the back contact of both samples. TEM measurement of devices with ordered absorbers did not show any distinguishable difference from the samples shown here, and are therefore not included. Based solely on the TEM measurements it is not possible to ascribe the Sn-rich regions to SnS_2. The device stack was therefore removed and the back contact and back side of the absorber were probed by Raman spectroscopy. Figure 6 shows the Raman spectra obtained from the Mo back contact after absorber removal. The modes at 288, 383, and 409 cm^{-1} can be ascribed to MoS_2 [37]. The modes at 205 and 314 cm^{-1} are ascribed to SnS_2 [38, 39, 40]. In Figure 5 the 13 min sample shows a strong presence of SnS_2 grains at the back contact. It is possible that these grains could act as a hole barrier if the density is sufficiently large. In our previous study SnS was found at the back contact [38]. The fact that SnS_2 is formed in this study indicates that the partial pressure of SnS_2(g) and sulfur was higher compared to our earlier work. It was observed

that SnS acts as an electron barrier at the front contact, but not as a hole blocking layer at the back contact [38]. Since the band gap of SnS_2 (about 2.1 - 2.3 eV [41, 39]) is much larger than SnS (1.1 - 1.3 eV [38, 42]), it is conceivable that large quantities of SnS_2 at the back contact could act as a barrier to hole transport.

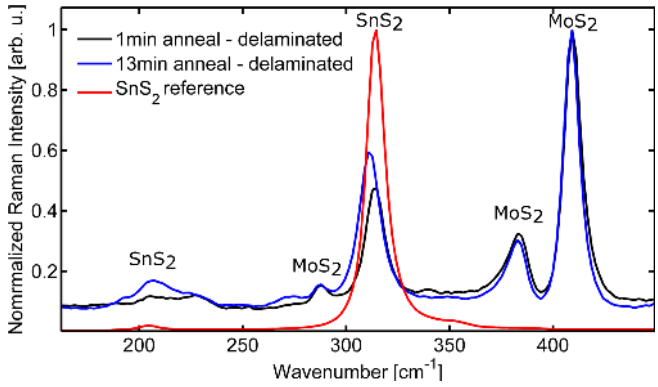

FIGURE 6 Raman scattering measured with a laser wavelength of 532 nm. The red spectrum is measured on a SnS_2 reference sample. The black and blue spectra are measured on the Mo back contact after absorber delamination of D1/CdS and D13/CdS.

In Figure 5 it is noticed that Cd has accumulated at grain boundaries and at the CZTS /MoS_2 interface. This is most clearly seen in the 13 min sample, but has also been observed in the 1 min sample. It is important to keep in mind that the devices were not heated after CdS deposition, so it seems likely that the Cd diffused into the grain boundaries during the 60 °C CBD process or during ZnO:Al sputtering. It is not common to observe Cd in the grain boundaries of CZTS, but it has been observed in nano-porous layers [43]. In that case it was argued that CdS aids passivation and collection from the grain boundaries. Whether Cd plays a similar role in these experiments cannot be concluded based on these results. It can, however, be ruled out that the Cd in-diffusion is the reason for the blocking behaviour seen in 13 min annealed samples, since the blocking is also observed for devices with ZTO buffer layers.

Even though the grains of the 1min annealed samples were significantly smaller, these devices had superior performance compared to the 13 min anneals. If grain boundaries are detrimental to the device operation, it would be expected that the 13 min anneals result in better performance. It could therefore appear that the grain boundaries are not detrimental, or to some extent passivated, as it has been suggested for CIGS [44]. The result is an indication that the quality of the grain interior (defect types and densities) might be more important than the density of grain boundaries at the current level of device performance. It is speculated that the high sulfur vapor pressure that is maintained in the short anneal is the key in improving the bulk properties.

4 | CONCLUSIONS

It is demonstrated that the band gaps of the CZTS bulk and its surface are very sensitive to the annealing conditions and thermal history of the material. Samples with a wide range of bulk band gaps can be obtained by variation of the annealing time and ordering of samples. It was demonstrated that both the surface composition and the valence band maximum was altered when exposing the samples to the ordering treatment. Furthermore, different buffer layers have been investigated with the goal to optimize the band alignment between buffer layer and absorber. A combination of

ZTO and a short annealing time resulted in a cell with an efficiency of 9.7%, which is the highest reported efficiency of CZTS with a Cd-free buffer layer. The results encourage further efforts to develop Cd-free buffer layers for CZTS. A high V_{OC} of 809 mV is demonstrated for ordered CZTS with a CdS buffer layer. Interestingly, the small grained CZTS resulting from a short 1 min annealing, yielded better devices than larger grained materials.

REFERENCES

[1] C. Yan, J. Huang, K. Sun, S. Johnston, Y. Zhang, H. Sun, A. Pu, M. He, F. Liu, K. Eder, L. Yang, J. M. Cairney, N. J. Ekins-Daukes, Z. Hameiri, J. A. Stride, S. Chen, M. A. Green, X. Hao, *Nat. Energy* **2018** , *3* , 764

[2] T. Minemoto, T. Matsui, H. Takakura, Y. Hamakawa, T. Negami, Y. Hashimoto, T. Uenoyama, *Sol. Energy Mater. & Sol. Cells* **2001** , *67* , 83–88

[3] M. Gloeckler, J. R. Sites, *Thin Solid Films* **2005** , *480-481* , 241–245

[4] D. Hauschild, D. Kreikemeyer-Lorenzo, P. Jackson, T. M. Friedlmeier, D. Hariskos, F. Reinert, M. Powalla, C. Heske, L. Weinhardt, *ACS Energy Lett.* **2017** , *2* , 2383–2387

[5] M. Morkel, L. Weinhardt, B. Lohmüller, C. Heske, E. Umbach, W. Riedl, S. Zweigart, F. Karg, *Appl. Phys. Lett.* **2001** , *79* , 4482–4484

[6] M. Bär, B.-A. Schubert, B. Marsen, R. G. Wilks, S. Pookpanratana, M. Blum, S. Krause, T. Unold, W. Yang, L. Weinhardt, C. Heske, H.-W. Schock, *Appl. Phys. Lett.* **2011** , *99* , 222105

[7] A. Santoni, F. Biccari, C. Malerba, M. Valentini, R. Chierchia, A. Mittiga, *J. Phys. D: Appl. Phys.* **2013** , *46* , 175101

[8] R. Haight, A. Barkhouse, O. Gunawan, B. Shin, M. Copel, M. Hopstaken, D. B. Mitzi, *Appl. Phys. Lett.* **2011** , *98* , 253502

[9] S. Englund, N. Saini, C. Platzer-Björkman, *Sol. Energy* **2018** , *175* , 84–93

[10] C. Yan, F. Liu, N. Song, B. K. Ng, J. A. Stride, A. Tadich, X. Hao, *Appl. Phys. Lett.* **2014** , *104* , 173901

[11] K. Sun, C. Yan, F. Liu, J. Huang, F. Zhou, J. A. Stride, M. Green, X. Hao, *Adv. Energy Mater.* **2016** , *6* , 1600046

[12] T. Ericson, F. Larsson, T. Törndahl, C. Frisk, J. Larsen, V. Kosyak, C. Hägglund, S. Li, C. Platzer-Björkman, *Sol. RRL* **2017** , *1* , 1700001

[13] C. Platzer-Björkman, C. Frisk, J. K. Larsen, T. Ericson, S.-Y. Li, J. J. S. Scragg, J. Keller, F. Larsson, T. Törndahl, *Appl. Phys. Lett.* **2015** , *107* , 243904

[14] J. Lindahl, C. Hägglund, J. T. Wätjen, M. Edoff, T. Törndahl, *Thin Solid Films* **2015** , *586* , 82–87

[15] F. Larsson, N. S. Nilsson, J. Keller, C. Frisk, V. Kosyak, M. Edoff, T. Törndahl, *Prog. Photovoltaics: Res. Appl.* **2017** , *25* , 755–763

[16] X. Cui, K. Sun, J. Huang, C.-Y. Lee, C. Yan, H. Sun, Y. Zhang, F. Liu, M. A. Hossain, Y. Zakaria, L. H. Wong, M. Green, B. Hoex, X. Hao, *Chem. Mater.* **2018** , *30* , 7860–7871

[17] Y. Ren, N. Ross, J. K. Larsen, K. Rudisch, J. J. Scragg, C. Platzer-Björkman, *Chem. Mater.* **2017** , *29* , 3713–3722

[18] J. J. S. Scragg, L. Choubrac, A. Lafond, T. Ericson, C. Platzer-Bjorkman, *Appl. Phys. Lett.* **2014** , *104* , 041911

[19] J. J. Scragg, J. K. Larsen, M. Kumar, C. Persson, J. Sendler, S. Siebentritt, C. Platzer Björkman, *physica status solidi (b)* **2015** , *253* , 189

[20] M. Grossberg, J. Krustok, T. Raadik, M. Kauk-Kuusik, J. Raudoja, *Curr. Appl. Phys.* **2014** , *14* , 1424–1427

[21] C. Malerba, M. Valentini, A. Mittiga, *Sol. RRL* **2017** , *1* , 1700101

[22] J. K. Larsen, J. J. Scragg, C. Frisk, Y. Ren, C. Platzer-Björkman, *physica status solidi (a)* **2015** , *212* , 2843–2849

[23] J. Lindahl, U. Zimmermann, P. Szaniawski, T. Törndahl, A. Hultqvist, P. Salomé, C. Platzer-Björkman, M. Edoff, *IEEE J. Photovoltaics* **2013** , *3* , 1100–1105

[24] M. Richter, M. Hammer, T. Sonnet, J. Parisi, *Thin Solid Films* **2017** , *633* , 213–217

[25] X. X. Liu, J. R. Sites, *J. Appl. Phys.* **1994** , *75* , 577–581

[26] T. Gokmen, O. Gunawan, T. K. Todorov, D. B. Mitzi, *Appl. Phys. Lett.* **2013** , *103* , 103506

[27] C. J. Hages, N. J. Carter, R. Agrawal, *J. Appl. Phys.* **2016** , *119* , 014505

[28] S. Siebentritt, *Sol. Energy Mater. Sol. Cells* **2011** , *95(6)* , 1471–1476

[29] A. Davydova, K. Rudisch, J. J. S. Scragg, *Chem. Mater.* **2018** , *30* , 4624–4638

[30] J. J. Yeh, I. Lindau, *At. Data Nucl. Data Tables* **1985** , *32* , 1–155

[31] T. Gleim, C. Heske, E. Umbach, C. Schumacher, S. Gundel, W. Faschinger, A. Fleszar, C. Ammon, M. Probst, H. P. Steinrück, *Surf. Sci.* **2003** , *531* , 77–85

[32] K. Timmo, M. Kauk-Kuusik, M. Pilvet, T. Raadik, M. Altosaar, M. Danilson, M. Grossberg, J. Raudoja, K. Ernits, *Thin Solid Films* **2017** , *633* , 122–126

[33] R. Ribeiro-Andrade, S. Sahayaraj, B. Vermang, M. R. Correia, S. Sadewasser, J. C. González, P. A. Fernandes, P. M. P. Salomé, *IEEE J. Photovoltaics* **2019** , 1–6

[34] F. Biccari, R. Chierchia, M. Valentini, P. Mangiapane, E. Salza, C. Malerba, C. L. A. Ricardo, L. Mannarino, P. Scardi, A. Mittiga, *Energy Procedia* **2011** , *10* , 187–191

[35] K.-J. Yang, J.-H. Sim, B. Jeon, D.-H. Son, D.-H. Kim, S.-J. Sung, D.-K. Hwang, S. Song, D. B. Khadka, J. Kim, J.-K. Kang, *Prog. Photovoltaics: Res. Appl.* **2015** , *23* , 862–873

[36] K. Wang, O. Gunawan, T. Todorov, B. Shin, S. J. Chey, N. A. Bojarczuk, D. Mitzi, S. Guha, *Appl. Phys. Lett.* **2010** , *97* , 143508

[37] J. M. Chen, C. S. Wang, *Solid State Commun.* **1974** , *14* , 857–860

[38] Y. Ren, M. Richter, J. Keller, A. Redinger, T. Unold, O. Donzel-Gargand, J. J. S. Scragg, C. Platzer Björkman, *ACS Energy Lett.* **2017** , *2* , 976–981

[39] L. S. Price, I. P. Parkin, A. M. E. Hardy, R. J. H. Clark, T. G. Hibbert, K. C. Molloy, *Chem. Mater.* **1999** , *11* , 1792–1799

[40] C. Julien, H. S. Mavi, K. P. Jain, M. Balkanski, C. Perez-Vicente, J. Morales, *Mater. Sci. Eng. B* **1994** , *23* , 98–104

[41] L. Burton, T. Whittles, D. Hesp, W. Linhart, J. Skelton, B. Hou, R. Webster, G. O'Dowd, C. Reece, D. Cherns, D. Fermin, T. Veal, V. Dhanak, A. Walsh, *J. Mater. Chem. A* **2016** , *4* , 1312–1318

[42] R. E. Banai, M. W. Horn, J. R. S. Brownson, *Sol. Energy Mater. Sol. Cells* **2016** , *150* , 112–129

[43] M. Werner, D. Keller, S. G. Haass, C. Gretener, B. Bissig, P. Fuchs, F. La Mattina, R. Erni, Y. E. Romanyuk, A. N. Tiwari, *ACS Appl. Mater. & Interfaces* **2015** , *7* , 12141–12146

[44] Y. Yan, C.-S. Jiang, R. Noufi, S.-H. Wei, H. R. Moutinho, M. M. Al-Jassim, *Phys. Rev. Lett.* **2007** , *99* , 235504